Biogeosciences Discuss., 10, 1111–1145, 2013
www.biogeosciences-discuss.net/10/1111/2013/
doi:10.5194/bgd-10-1111-2013

Biogeosciences Discussions

Numerical modelling of methyl iodide in the Eastern Tropical Atlantic

I. Stemmler[1], **M. Rothe**[1,*], **and I. Hense**[1]

[1]Institute for Hydrobiology and Fisheries Science, CEN, University of Hamburg, Hamburg, Germany
[*]now at: Leibniz Institute of Freshwater Ecology and Inland Fisheries, Berlin, Germany

Received: 19 December 2012 – Accepted: 11 January 2013 – Published: 24 January 2013

Correspondence to: I. Stemmler (irene.stemmler@zmaw.de)

Published by Copernicus Publications on behalf of the European Geosciences Union.

Abstract

Methyl iodide (CH_3I) is a volatile organic halogen compound that contributes significantly to the transport of iodine from the ocean to the atmosphere, where it plays an important role in tropospheric chemistry. CH_3I is naturally produced and occurs in the global ocean. The processes involved in the formation of CH_3I, however, are not fully understood. In fact, there is an ongoing debate whether production by phytoplankton or photochemical degradation of organic matter is the main source term. Here, both the biological and photochemical production mechanisms are considered in a biogeochemical module that is coupled to a one-dimensional water column model for the Eastern Tropical Atlantic. The model is able to reproduce observed subsurface maxima of CH_3I concentrations. But, the dominating source process cannot be clearly identified as subsurface maxima can occur due to both, direct biological and photochemical production. However, good agreement between the observed and simulated difference between surface and subsurface methyl iodide concentrations is achieved only when direct biological production is taken into account. Published production rates for the biological CH_3I source that were derived from laboratory studies are shown to be inappropriate for explaining CH_3I concentrations in the Eastern Tropical Atlantic.

1 Introduction

Methyl iodide (CH_3I) is one main carrier of iodine from the ocean to the atmosphere (Lovelock et al., 1973). Upon volatilization to the atmosphere it rapidly (within 5 days) transforms into reactive iodine species and impacts the tropospheric chemistry, such as the oxidative capacity and ozone depletion (Chameides and Davis, 1980). In coastal regions macro-algae were identified as significant methyl iodide sources (Nightingale et al., 1995), but they are not the major producers on the global scale due to their restricted distribution and small production rates (Wang et al., 2009). In the open ocean CH_3I sources are unclear and uncertainties remain with regard to origin of the source

BGD
10, 1111–1145, 2013

as well as production rates. Most studies suggested either a biological or a photochemical production pathway. Laboratory experiments in which filtered seawater was irradiated show photochemical production of CH_3I in absence of living phytoplankton cells that could account for at least 50 % of observed CH_3I emissions from the tropical Atlantic (Richter and Wallace, 2004). In addition, there is direct evidence for the biological production pathway; in particular the picocyanobacteria *Prochlorococcus* produce CH_3I (Brownell et al., 2010). The CH_3I production rates that have been independently derived for the same species by different research groups, however, are several orders of magnitude apart (Smythe-Wright et al., 2006; Brownell et al., 2010). While it was unclear whether differences in experimental setups in these laboratory studies can explain the discrepancies, a very recent work provides an alternative explanation. Apparently, the production of methyl iodide is related to the health of these unicellular organisms; enhanced production rates by an order of magnitude have been recorded under stress conditions (Hughes et al., 2011). So far, only in few modeling studies oceanic CH_3I production have been quantified. Based on a very limited data set, best agreement between observations and model results from global chemistry-transport model (Bell et al., 2002) have been obtained when considering only a photochemical source instead of biological production. However, it has been criticized that the simulated photochemical source being too strong and the parametrization possibly too crude to represent CH_3I production (Moore, 2006). Since then more data on CH_3I in the environment have been collected and new insights in CH_3I production published. The existing uncertainties show the need to readdress the origin of oceanic CH_3I applying recent process understandings. Here, we present results from model experiments in which both the biological and photochemical production mechanisms are considered. We compare model simulated concentrations of CH_3I with observations in order to assess distribution and strength of natural CH_3I sources in the ocean. A methyl iodide source and sink module is developed and coupled to a biogeochemical model as well as to the water column model GOTM. This model system is applied to simulate CH_3I concentrations in the Eastern Tropical Atlantic. By comparing observed and simulated

BGD
10, 1111–1145, 2013

vertical profiles of methyl iodide, we aim at identifying possible sources and sinks. Additionally, we want to quantify the air-sea flux of CH_3I and determine the sensitivity of this exchange process towards different parameterization for CH_3I production.

2 Material and methods

2.1 Model description

The physical model used is the "General Ocean Turbulence Model" (GOTM, Umlauf et al., 2005). GOTM is a one dimensional water column model that mimics a number of hydrodynamic and thermodynamic processes related to vertical mixing in natural waters. It derives solutions for the one-dimensional versions of the transport equations of momentum, salt and heat and includes well-tested turbulence models. These models span the range from simple prescribed expressions for the turbulent diffusivities up to complex Reynolds-stress models with several differential transport equations to solve.

Phytoplankton dynamics are simulated using a single column implementation of HAMOCC (Six and Maier-Reimer, 1996; Wetzel et al., 2006). HAMOCC is a marine carbon cycle model that includes an NPZD-type ecosystem model. The latter resolves exchange processes between several compartments: phytoplankton, zooplankton, sinking particulate organic carbon, a semi-labile dissolved organic carbon, and nutrients (iron, nitrate, and phosphate).

2.1.1 Methyl iodide modelling

The methyl iodide module considers several source and sink processes of CH_3I and has been implemented into the biogeochemical module HAMOCC. The methyl iodide concentration (c [mmol m^{-3}]) evolves over time following production (P), degradation (S), air-sea exchange (F), as well as turbulent vertical diffusion (A_v-diffusion

BGD
10, 1111–1145, 2013

coefficient).

$$\frac{dc}{dt} = P - S + F_{\text{air–sea}} + \frac{\partial}{\partial t}\left(A_v \frac{\partial c}{\partial z}\right) \quad (1)$$

Two production mechanisms are implemented: photochemical production by radical recombination between methyl groups and iodine atoms (P_{photo}) and direct biological production by phytoplankton (P_{PP}). Photochemical production is parameterized using the photosynthetically active radiation PAR and a dissolved organic carbon concentration DOC. Here, PAR triggers the formation of methyl groups in the presence of organic mattter and the production of iodine atoms from the photolysis of organic iodide. The change of methyl iodide concentration over time is then parameterized as follows:

$$P_{\text{photo}} = k_{\text{photo}} \cdot \text{PAR} \cdot \text{DOC} \quad (2)$$

where k_{photo} is the photchemical production rate in $\text{m}^2\,\text{mmol}\,\text{CH}_3\text{I}\,(\text{kmol}\,\text{P})^{-1}\,\text{W}^{-1}\,\text{s}^{-1}$. The term DOC gathers a large variety of different substances with very different properties of different origin, as "dissolved" is an operational definition for material passing a 0.45 µm filter. DOC can be directly produced in the ocean or orginate from terrigenous decomposed plant material. Marine processes that form DOC include mainly extracellular release by phytoplankton, grazer mediated release and excretion, release via cell lysis, solubilization of particles, and bacterial transformation and release (Carlson, 2002). Relevant for CH_3I production are the DOC's photochemical properties, i.e. its ability to release methyl radicals. Photochemical transformation thereby can change the bioavailability of DOC in both directions, i.e. can make it more recalcitrant or more bioavailable (Sulzberger and Durisch-Kaiser, 2009). To cover DOC pools of different lability two types of experiments with photochemical production of CH_3I are performed. In one group of experiments the semil-labile DOC (SLDOC) pool of pure marine origin as provided by HAMOCC is used as a source for methyl groups. In the experiments that mimic a biologically refractory pool of DOC (RDOC) as the source of methyl groups, the DOC concentration is set to a constant value of 40 µmol C kg^{-1}. This is reasonable, as

BGD
10, 1111–1145, 2013

the concentration of refractory DOC can be considered constant at the surface where photochemistry takes part (Carlson, 2002).

Direct biological production of CH_3I by phytoplankton is parameterized as follows:

$$P_{PP} = k_{PP} \cdot \mu(T, N, \mathrm{PAR}) \cdot P \tag{3}$$

Here, P is the phytoplankton concentration in kmol P m^{-3} and $\mu(T, N, \mathrm{PAR})$ is the actual growth rate of phytoplankton. The coefficient that specifies how much methyl iodide is produced during primary production is called ratio k_{PP} [mmol CH_3I (kmol P)$^{-1}$]. This proportionality coefficient has been derived from two different laboratory studies: Moore et al. (1996) conducted incubation experiments with the phytoplankton species *Nitzschia* sp. and Smythe-Wright et al. (2006) incubated the cyanobacteria species *Prochlorococcus marinus*. Both measured an increase of methyl iodide concentration during the exponential growth phase of phytoplankton. In order to determine this coefficient, first the maximum specific growth rates ω in d^{-1} of these two species have been extracted from the exponential growth phase. The observed change in cell abundance is a function of the actual (net) growth rate μ. Since, the maximum specific growth rate is required (see also Hense and Quack, 2009) a respiration rate of 1 % d^{-1} is assumed. Solving the ordinary differential equation for the experiment explained above

$$\frac{dP}{dt} = \mu \cdot P \tag{4}$$

and rearrange it to solve for μ

$$\mu = \frac{\ln\left(\frac{P}{P_0}\right)}{\Delta t} \tag{5}$$

the phytoplankton production within Δt is

$$\text{Phytoplankton production} = \omega \cdot P_0 \cdot e^{\omega \cdot \Delta t} \tag{6}$$

BGD
10, 1111–1145, 2013

with P_0 and P accounting for the cell counts at the beginning and the end of the exponential growth phase, the time interval Δt and $\omega = \mu + 0.01\,\mathrm{d}^{-1}$. Then the corresponding change of methyl iodide concentration ΔCH_3I in the same time interval Δt is determined in order to calculate the ratio between methyl iodide production and primary production k_{PP}

$$k_{PP} = \frac{\text{Methyl iodide production}}{\text{Phytoplankton production}} = \frac{\Delta CH_3I}{\Delta t \cdot \omega \cdot P_0 \cdot e^{\omega \cdot \Delta t}} \tag{7}$$

The resulting values for k_{PP} are $0.1232\,\mathrm{mmol\,CH_3I\,(kmol\,P)^{-1}}$ for *Nitzschia* sp. and $1488.00\,\mathrm{mmol\,CH_3I\,(kmol\,P)^{-1}}$ for *Prochlorococcus marinus*, using typical cellular carbon contents for both species (Partensky et al., 1999: $50\times10^{-15}\,\mathrm{g\,C\,cell^{-1}}$ for *Prochlorococcus marinus*; $147\times10^{-12}\,\mathrm{g\,C\,cell^{-1}}$ for *Nitzschia* sp. see also Hense and Quack, 2009) as well as the conversion from weight to molar units and the molar Redfield ratio ($P:C = 1:106$). Under stress conditions the ratio between primary production and production of organic halogens significantly increases (Hughes et al., 2011). As picocyanobacteria are very abundant in the oligotrophic ocean (Partensky et al., 1999), and a large fraction of cells is in an unhealthy state (Agusti, 2004), we take nutrient limitation N_{lim} as a simple proxy for picocyanobacteria and for stress conditions to identify possible unhealthy cell states of phytoplankton:

$$N_{lim} = \frac{N}{N + k_N} \tag{8}$$

where N is the nutrient concentration and k_N the half saturation rate for nutrients. When enhanced production under nutrient limitation is simulated, k_{PP} varies between a minimum value under nutrient-rich conditions ($N_{lim} = 0.999$) and a maximum value under extremly oligotrophic conditions ($N_{lim} = 0.001$):

$$k_{PP} = a \cdot \exp(-bN_{lim}) \tag{9}$$

BGD
10, 1111–1145, 2013

with

$$b = \frac{\ln\left(\frac{k_{PP_{min}}}{k_{PP_{max}}}\right)}{0.001 - 0.999} \tag{10}$$

and

$$a = \frac{k_{PP_{max}}}{\exp(-b \cdot 0.001)} \tag{11}$$

This non-linear approach was chosen to test the sensitivity versus minimum and maximum values of k_{PP} which can span several orders of magnitude. A linear approach here would over-represent the high values.

CH_3I degradation includes nucleophilic substitution with chloride S_{Cl}, hydrolysis S_{hyd}, and photolysis S_{phot}. Chloride substitution and hydrolysis are implemented as first order processes with temperature dependent decay rates:

$$S_{Cl} = k_{Cl}(T) \cdot c_{Cl} \cdot c \tag{12}$$

and

$$S_{hyd} = k_{hyd}(T) \cdot c \tag{13}$$

For chloride substitution a constant chloride ion sea water concentration of $c_{Cl} = 0.54\,\mathrm{mol\,L^{-1}}$ was adopted, which is a typical value when assuming a mean sea water salinity $S = 35$ and a chloride ion proportion of 55 % (following the law of constant proportions after Dittmar, 1884). The reaction rate was derived by Elliott and Rowland (1993)

$$k_{Cl} = A \cdot \exp\left(-\frac{B}{T}\right) \tag{14}$$

BGD
10, 1111–1145, 2013

with $A = 7.78 \times 10^{13}\,\mathrm{L\,mol^{-1}\,s^{-1}}$, and $B = 13518\,\mathrm{K}$, T – temperature in K. The reaction rates for hydrolysis were determined by Elliott and Rowland (1995) with $A = 1.7 \times 10^{12}\,\mathrm{s^{-1}}$, and $B = 13300\,\mathrm{K}$. Photolysis is implemented as proportional to UV attenuation a_{uv}, and irradiance (I) relative to its annual mean I_{ref}:

$$S_{\mathrm{photo}} = k_{\mathrm{uv}} \cdot \frac{I}{I_{\mathrm{ref}}} \exp(-a_{\mathrm{uv}} z) \tag{15}$$

The rate constant k_{uv} [$\mathrm{s^{-1}}$] is estimated from atmospheric degradation rates (Rattigan et al., 1997), because reaction kinetics of methyl iodide photolysis in seawater are unknown. In particular, the e-folding time $(k_{\mathrm{uv}})^{-1}$ is set to 10 days assuming photodissociation of methyl iodide in water occurs at 50 % of the respective atmospheric rate. This approach was adopted from Carpenter and Liss (2000) who estimate kinetics of bromoform photolysis in water in a similar manner.

Gas exchange is calculated from the two-film model assuming methyl iodide gas exchange is controlled by the water side due to its low water solubility. Hence, the flux is calculated from a time-invariant field of atmospheric concentrations, solubility (Henry's law constant), bulk surface water concentrations, the Schmidt number, and a transfer velocity.

$$F_{\mathrm{air\text{–}sea}} = k_{\mathrm{w}} \cdot \left(c - \frac{c_{\mathrm{a}}}{H} \right) \tag{16}$$

The transfer velocity k_{w} depends on wind speed and is calculated according to Nightingale et al. (2000)

$$k_{\mathrm{w}} = \left(6.16 \times 10^{-7}\,\mathrm{s\,m^{-1}} \cdot u_{10}^2 + 9.25 \times 10^{-7} u_{10} \right) \left(\frac{Sc_{\mathrm{CH_3I}}}{600} \right)^{-\frac{1}{2}} \tag{17}$$

with u_{10} denoting the wind speed at 10 m above the sea surface and $Sc_{\mathrm{CH_3I}}$ the Schmidt number for methyl iodide. The Schmidt number has been estimated from that of methyl

BGD
10, 1111–1145, 2013

bromide and the ratio of their molar volumes, as it has been done previously (e.g. Moore and Groszko, 1999)

$$Sc_{CH_3I} = \left(\frac{62.9}{52.9}\right)^{0.6} \cdot \left(2004 - 93.5\,°C^{-1} \cdot T + 1.39\,°C^{-2} \cdot T^2\right) \quad (18)$$

with T temperature in °C (5 °C–30 °C). The temperature dependence of the solubility was determined by Moore et al. (1995):

$$H = \exp\left(13.32 - \frac{4338\,K}{T}\right) \quad (19)$$

with T temperature in K.

2.2 Model setup

In order to receive a realistic simulation for a given oceanic region the model has to be configured for the conditions in a specific region. In this study, GOTM is configured for the Cape Verde region in the eastern tropical North Atlantic Ocean (Latitude: 16° N, Longitude: 24° W), like in Hense and Quack (2009). The physical model covers the upper 700 m of the ocean and has a vertical resolution of 2 m. The lower boundary of the model is set at this depth because here the nutrient maximum occurs and all diffusive fluxes vanish. A two-equation k-ε model with an algebraic second momentum closure is used which is similar to Weber et al. (2007). For numerical integration a so called quasi- implicit numerical scheme for the turbulence model with a time step of 1 h is used. The coupled physical biogeochemical model is forced by climatological monthly mean data of 2 m atmospheric air temperature, air pressure, dew point temperature, 10 m zonal and meridional wind velocities, cloud cover and precipitation. The variables for water temperature and salinity are initialized with climatological profiles from the World Ocean Atlas (WOA01) (Conkright et al., 2002). The NPZD model parameters were tuned to closer match conditions at Cape Verde (see Appendix and Table 1).

BGD
10, 1111–1145, 2013

For the calculation of the air-sea gas exchange a constant methyl iodide air concentration of 6.23×10^{-8} mmol m^{-3} is assumed which corresponds to 1.5 ppt at 20 °C and is the mean of observed base level air concentrations of methyl iodide at Cape Verde during May and June 2007 (O'Brien et al., 2009). To account for lateral entry of higher saline water, which is characteristic for the Cape Verde region, salinity and temperature values are restored towards climatological monthly means of WOCE (World Ocean Circulation Experiment; Global Data Resource) with a five day timescale, except for the upper 20 m of the water column. The dissolved inorganic nitrogen concentration is restored at the nutrient maximum to the observed value of 35.7 mmol N m^{-3}, and dissolved inorganic phosphate to an observed value of 2.23 mmol P m^{-3} with a time scale of one hour.

GOTM is run in several experiments including different combinations of the CH_3I production processes (listed in Table 2). In the experiments E1 and E2 only direct production via phytoplankton growth is implemented and the production rates derived from laboratory studies by Moore et al. (1996) (E1) and Smythe-Wright et al. (2006) (E2) are tested. In experiment E3 the production rates by Moore et al. (1996) and Smythe-Wright et al. (2006) are used as the lower and upper boundaries of the variable biological production rate that mimics production by phytoplankton with consideration of stress. As the production rates for the photochemical production pathways (from SLDOC or RDOC) are unknown they are derived from a parameter optimization. Thereby the parameter (set) that leads to the minimum root mean square deviation (RMSD):

$$\mathrm{RMSD} = 0.5\sqrt{\frac{1}{N_{\mathrm{depth}}}\sum_{\mathrm{depth}}(m_{\mathrm{depth}} - o_{\mathrm{depth}})^2} + 0.5\sqrt{(\max(m) - \max(o))^2} \quad (20)$$

between modelled (m) and observed (o) (see Sect. 2.3) profiles and maxima is found using a gradient descent search. The step length, i.e. the incremental parameter change, is set to 10 % of the most successful parameter value of the previous iteration. Optimizing for both, the overall RMSD and the deviation from the maximum,

BGD
10, 1111–1145, 2013

ensures that when a subsurface maximum is simulated it will be of similar strength as in the observations, even when predicted at a different depth. The experiments Opt1–Opt4 include only one source process and the parameters are chosen by a parameter optimization. In the following, 1 denotes "normal" (not stressed) production by phytoplankton, 2 photochemical production through semilabile DOC (SLDOC) degradation, 3 photochemical production through refractory DOC (RDOC) degradation, and 4 biological production with a variable production rate (i.e. with consideration of stress), where the lower and upper bounds are optimized. In the experiment Opt123, three production processes are considered (i.e. biological and photochemical production from semi-labile and refractory DOC), and the respective rates are derived from a parameter optimization with three simultaneously varying parameters.

2.3 Observations

To evaluate the simulated CH_3I concentrations model results are compared to observations from a ship cruise in the tropical Northeast Atlantic close to Cape Verde, i.e. the *Poseidon Cruise* P399 in April–June 2010 (Bange, 2011). Methyl iodide profiles are available from three stations located at 18° N 17° W (St.311), 17.6° N 24.3° W (St.307 – in the following called TENATSO, which stands for Tropical Eastern North Atlantic Time-Series Observatory), and 18° N 21° W (St.308). At TENATSO the profile includes the water depths 10.7, 40.6, 60.9, 80.7, 101, 151, 509, 1108, 2021, 3038 m. At St.308 water was collected at 12.1, 22.8, 43, 53.5, 67.8, 81.9, 101.6, 152.2, 202.9, and 302.8 m. At St.311 the profile includes data from 10.1, 24.2, 44.1, 63.9, 104.1, 154.6, and 305.3 m below the sea surface. Besides methyl iodide concentrations phytoplankton pigments, temperature, and salinity profiles are available for the three stations. Phytoplankton pigments, i.e. total chlorophyll *a* concentrations, were converted into phytoplankton biomass by using a depth dependent C : Chl ratio and assuming a $P:C$ ratio of 1 : 106. The C : Chl ratio was calculated as described in Hense and Beckmann (2008) using modelled radiation profiles, as these were not measured for

BGD
10, 1111–1145, 2013

the three stations. Calculated surface C : Chl ratios are much higher ($> 100\,g\,g^{-1}$) than subsurface (minimum $25\,g\,g^{-1}$) ratios (not shown).

3 Results

3.1 Seasonal cycle of CH_3I concentrations

In the experiments that include only biological production of CH_3I (Opt1, E1, E2) maximum production takes place between 50 and 80 m depth, i.e. where phytoplankton growth is largest (Fig. 1a). Consequently, a strong CH_3I subsurface maximum builds up over the year, with highest concentrations in the summer season (May–September). The experiments that include photochemical production show a subsurface CH_3I maximum, too. But, location and cause of this maximum are different from the experiments with biological production. Irrespective of the lability of the DOC pool considered, maximum CH_3I production occurs in the sun-lit surface layers (Fig. 1c, d). The production is stronger in summer than in winter months, following the seasonal cycle of insolation. During times of deep mixing, i.e. in winter months, the CH_3I concentration is homogenous over the upper 50 m. When the mixed layer shallows, a pronounced subsurface maximum evolves, which is first situated at approx. 50 m depth, but later follows the mixed layer shallowing up to approx. 30 m depth. In the uppermost model levels the dominant sink processes for CH_3I are UV decay and gas exchange with the atmosphere. The subsurface maximum is not a result of a particularly strong local production (production always exeeds decay), but is caused by the stratification that shields the freshly produced CH_3I from gas exchange. The experiments Opt2 and Opt3, show only minor differences, despite the different DOC pools considered as sources for available methyl groups. This is because the semi-labile DOC in HAMOCC shows a surface maximum throughout the year. Hence, the vertical distribution of CH_3I production in both experiments is limited by light absorption leading to similar seasonal patterns.

BGD
10, 1111–1145, 2013

In Opt4, when biological production is simulated and calculated from different production rates in oligotropic water and the residual water column, the distribution of CH_3I differs very much from that of "normal" biological production in, e.g. Opt1 (Fig. 1d). Concentration maxima occur from May to September and stretch within the upper 40 m of the water column. Production is highest at the surface, because nutrient scarcity (caused by strong stratification of the water) leads to a high CH_3I : PP ratio k_{PP} (Fig. 2). At the surface k_{PP} is 4–6 times higher than in Opt1 and is more than 100 times lower than in Opt1 subsurface where maximum primary production occurs (Fig. 2a). The distribution of CH_3I in Opt123 is almost identical to Opt2 and Opt3, because as a result of the optimization k_{PP} is even smaller than in E1 (Table 2), the experiment with the low biological production rate dervied from laboratory experiments.

3.2 Evaluation of simulated CH_3I concentrations

In the experiments E1 and E2, i.e. when considering only biological production using the rates derived from laboratory studies (Table 2), different concentration distributions evolve resulting from the balance between production, degradation and gas-exchange with the atmosphere. Though in both experiments CH_3I production is tied to primary production, and hence is highest at the subsurface maximum of phytoplankton growth, only in E2 a subsurface CH_3I concentration maximum appears (similar to Opt1 in Fig. 1a). In E1 production and therefore surface concentration are very low. This leads to an undersaturation of the ocean and a net influx of CH_3I from the atmosphere throughout the year, highest in the more windy winter, spring and fall seasons (not shown). Consequently, CH_3I concentrations in E1 are highest at the surface, during winter, spring, and fall and lowest in summer. During times of a deep mixed layer CH_3I is mixed down to 50 m depth, whereas in summer when the ocean is strongly stratified, the gas stays in the surface layer and is photolysed. In comparison to observed profiles, the model overestimates CH_3I concentrations in E2 and underestimates them in E1. The observed maximum and mean concentrations are 5.66, 1.49 pmol L^{-1} at TENATSO and 3.34, 0.66 pmol L^{-1} at St.308 (Table 3). The model in turn predicts for

BGD
10, 1111–1145, 2013

the respective month maximum and mean concentrations of 0.11, 0.02 pmol L^{-1} in E1 and 173.2, 60.67 pmol L^{-1} in E2 for TENATSO, and 0.14, 0.004 pmol L^{-1} in E1 and 187.65, 70.43 pmol L^{-1} in E2 for Stat.308. Only the surface value of E1 matches the observations at Stat.308 within a factor of 2. But, this apparent match is insignificant considering the large discrepancy (between observations and E1 model results) in subsurface concentrations. Mean and maximum values in E3, the experiment that allows for a variable biological CH_3I production rate using the parameters from laboratory studies as lower and upper bounds, match observed mean and maximum values much better (i.e. within a factor of 2) than the ones of E1 and E2. But, the vertical profile differs from the observed one: the strong production at the surface leads to concentrations that are much too high (100 times compared to TENATSO, 6 fold compared to Stat.308, see Table 3).

For "normal" biological production, photochemical production (from RDOC and SLDOC), biological production with a variable k_{PP}, and combined biological and photochemical production a parameter optimization towards observed profiles at TENATSO was performed. Assuming that differences between TENATSO and Stat.308 are minor, no individual optimization for Stat.308 was performed. For the experiment with mixed sources (Opt123) the optimization results in a very low biological production rate k_{PP} (Table 2), and consequently in a dominance of the photochemical production pathways. Therefore, the methyl iodide concentration evolves similar to Opt2 and Opt3 (Fig. 1b, c).

Results of the experiments using optimized parameter values compared to observations are depicted in a Taylor diagram (Fig. 3). It shows the RMSD (Eq. 20) normalized to the observed mean concentration at TENATSO and St.308 (Fig. 3), the standard deviation across the profile normalized to the profiles' mean concentration, and the correlation coefficient between modelled and observed profile. Of course, correlation and standard deviation are weak measures for the match between model and observations here, due to the low data resolution. Nevertheless, they can give a hint on the similarity of the shapes of modelled and observed profiles. The temporal evolution of CH_3I

BGD
10, 1111–1145, 2013

concentration can not be evaluated at all, because there are no long-term CH_3I data that would allow for assessing the seasonal cycle in the Eastern Tropical Atlantic. Observed methyl iodide concentrations show a subsurface maximum at around 40–50 m at both Stations (Fig. 4). Due to the parameter optimization all of the experiments simulate CH_3I concentrations that are close to the observed maximum and mean values at TENATSO, and match observed profiles much better than E1 and E2 (see Table 3). At TENATSO the maximum concentration and concentrations below the maximum are well represented in almost all experiments, except Opt4 (Fig. 4). In the Taylor diagram Opt2,Opt3, and Opt123 are clustered closely at approximately the same distance from the observations, as their profiles are very much alike (Fig. 4). According to the Taylor diagram (Fig. 3a) Opt1 is closest to the observations, as it is the only experiment that reproduces the subsurface gradient of the observations, driven by a low surface concentration. This translates into a higher correlation coefficient and a lower RMSD. Surface concentrations of the experiments that are dominated by photochemical production (Opt2, Opt3, Opt123) are too high compared to observations (Fig. 4, Table 3). For Opt4, the optimization converged to values that are not very different from the values at E3 (Table 2) and the representation of methyl iodide in that model experiment did not improve much over the ones in E3, too. Compared to TENATSO, most simulated vertical profiles show a too shallow maximum, with too low values below and too high surface values. Observations at Stat.308 are generally worse represented by this model setup than observations at TENATSO. A further parameter optimization would bring simulated concentrations closer to observed ones, but would not bring any further insights into CH_3I production. Also here (at Stat.308) it is apparent, that the experiment with CH_3I production by phytoplankton (Opt1) is the only one that can reproduce the sharp subsurface gradient of the observations, when all others show rather high surface concentrations compared to the subsurface maximum (Fig. 4, Table 3).

BGD
10, 1111–1145, 2013

3.3 Emissions

In all experiments with optimized production rates the ocean acts as a source of CH_3I to the atmosphere. Flux maxima for most experiments but Opt1 occur in spring (March–May, Fig. 5), due to high surface ocean concentrations during these times. In Opt1 highest emissions occur in winter (December, January, February), when both CH_3I production at the surface (Fig. 1a) and wind speed (Fig. 5) are high. The fluxes are of similar order of magitude for all experiments (maxima at approx. 500 $pmol\,m^{-2}\,h^{-1}$). The primary driver of direction and annual cycle of gas exchange is the concentration of CH_3I in the surface layer of the model. Hence, the ultimate reason for the difference among the experiments is that biological production is at its maximum in the ocean interior (at ca. 60 m) in summer, and at the surface in winter, whereas photochemical production is highest in the sun-lit surface layers during spring and summer. When production is limited to photochemical production the seasonal cycle of the gas exchange is less pronounced (Fig. 5). This is because the temporal evolution of production is controlled by radiation, and hence strongest in summer, when low wind speeds lead to a lower transfer velocity. Besides by production and associated surface concentrations, the evolution of the fluxes is determined by wind speed and sea surface temperature. The low temporal resolution of wind speed (monthly means) via the transfer velocity shapes the month-to-month variation of the fluxes, which is characterized by an abrupt (non-smooth) transition from one month to the other (Fig. 5). Within individual months temperature, which determines the solubility, and surface concentration control the deviation from equilibrium between atmosphere and ocean, and hence the evolution of sea-air fluxes.

4 Discussion

The profiles of temperature, salinity, phytoplankton, and nutrients at TENATSO and St.308 during P399 are similar to observations in Meteor cruise M55 (Wallace and

BGD
10, 1111–1145, 2013

Bange, 2004) and the World Ocean Atlas (Conkright et al., 2002), hence the observed profiles at these stations do not represent unusual environmental conditions. Therefore it seems reasonable to conclude from the findings of the current study on methyl iodide behaviour in parts of the Tropical Eastern Atlantic that are not directly affected by coastal upwelling.

Modelling CH_3I distributions at TENATSO and St.308 using biological production rates derived from laboratory experiments (E1, E2) was not successful. The production rate as suggested by Moore et al. (1996) appears to be too low to reproduce observed CH_3I concentrations, whereas the production rate suggested by Smythe-Wright et al. (2006) seems to be too high. This does not imply that direct biological production of methyl iodide is unlikely. The parameter optimization for the cases where only biological production was included (Opt1) resulted in lowest RMSD values for a production rate in the order of magnitude of −6 and best reproduced the overall shape of the vertical profiles. Hughes et al. (2011) suggested that the large discrepancies between the production rates from laboratory studies result from the different health conditions of the phytoplankton cells. As in reality the phytoplantkton population can consist of mixed healthy and stressed cells (Agusti, 2004), it is not unrealistic to expect a bulk CH_3I production rate inbetween the two discussed. Here, we tested if enhanced production under oligotropic conditions would result in a better representation of CH_3I profiles close to Cape Verde. But, even after optimization of the parameter setup this experiment did not reproduce observed concentrations satisfactorily. The preliminary analysis of pigment measurements in the Cruise report (Bange, 2011) indicates a high abundance of diatoms, but also suggests the presence of *Prochloroccus* and *Syneococcus* during P399. Nothing is known about the cell physiological state of phytoplankton during the cruise. Hence, either nutrient scarcity is not a good proxy for stressed phytoplankton cells that produce more CH_3I than healthy ones and the chosen parameterisation of that factor is inadequate, or enhanced production by stressed cells is not relevant at these two stations. Erros in the physical or ecosystem model of course propagate leading to inaccurate methyl iodide concentrations. As for both stations the

BGD
10, 1111–1145, 2013

same physical setup of GOTM is used particularities of the two stations, e.g. if enhanced production by stressed picocyanobacteria would be more likely for St.308 than for TENATSO, are not reflected in the model and can not be discussed. The main features both stations and the model have in common are the existance of a subsurface phytoplankton and CH_3I maximum, the pronounced stratification in summer, and the vertical nutrient distribution. In particular in comparison to TENATSO the experiments that are dominated by photochemical production are very successfull in representing the subsurface CH_3I concentrations (below the maximum), and only the surface value is not represented by the model. As the optimization is set-up to find the minimum RMSD for both maximum and mean along the profile, the discrepancy in the surface value is not weighted strongly enough to force the mixed source parameter optimization towards a biological production. Hence one can not conclude from the mere fact that the optimization suppressed biological production, that photochemical production is the main source process of CH_3I, here. As in oligotrophic waters deep phytoplankton maxima regularly occur higher biologically mediated methyl iodide production at depth can hence not be excluded. This is supported by Smythe-Wright et al. (2006), who found enhanced subsurface CH_3I concentrations where *Prochlorococcus* were largely abundant. Smythe-Wright et al. (2006) found much higher CH_3I concentrations during their cruise than found at Cape Verde during P399, although both were conducted in the same season. Smythe-Wright et al. (2006) found elevated surface concentrations as well as associated high atmospheric levels. Smythe-Wright et al. (2006) diagnose concentration anomalies of 40 pmol L^{-1} in May from data collected in the Eastern Atlantic close to 20° N, resulting from very high CH_3I concentrations in water. Concentrations measured during P399 and simulations show much lower values. The concentration anomaly between water and air of approx. 5–10 pmol L^{-1} modelled here is closer to what was estimated by Happell and Wallace (1996), Richter and Wallace (2004), or Chuck et al. (2005). Clearly, as model results were optimized for certain sea water concentrations, a direct comparison to other measured data is only possible when these coincide to the ones at P399. Chuck et al. (2005) for example, measured surface water

BGD
10, 1111–1145, 2013

concentration of approx. 5 pmol L^{-1} off Africa at 15–20° N, which is much higher than concentrations measured during P399. Generally, the strength modelled sea-air fluxes does not vary much among the experiments, but its seasonal cycle does. Even though the large differences in intensity of gas exchange for experiments that include different dominating source processes seems to be an inherent feature of production, the sea-air flux can not be used to argue for a certain source type. This is because in the model sea-air exchange is only diagnosed from a constant atmospheric concentration. Such argumentation can ony be done using a model that includes the full cycling of CH_3I in atmosphere and ocean.

5 Conclusions

The coupled biogeochemical-water column model that includes a methyl iodide compartment is able to reproduce observed subsurface maxima of CH_3I concentrations. However, our model results are not unequivocal. Subsurface maxima can occur due to direct biological and photochemical production. Thus, the source of CH_3I cannot be clearly identified. The gradient, i.e. the difference between surface and subsuface methyl iodide concentration is, however, best reproduced if direct biological production is taken into account. Although enhanced methyl iodide production is observed under stress conditions of picocyanobacteria, the parameterization of this process has not led to a model improvement at this particular site.

Overall, we conclude that the rates obtained from the laboratory experiments from Moore et al. (1996) are too low to explain the CH_3I concentration in the tropical Northeast Atlantic. In contrast the CH_3I production rates in this region cannot be as high as proposed by Smythe-Wright et al. (2006) at least not over longer times. The comparison of horizontal distribution patterns between simulated and observed CH_3I concentrations may provide further insights into the source of CH_3I.

BGD
10, 1111–1145, 2013

Appendix A

Evaluation of the physical and biological state of model

For all simulations the model was restored towards salinity and temperature profiles from the tropical Northeast Atlantic (see Sect. 2.2). But, this does not guarantee that the simulated ocean state is representing conditions during the Poseidon cruise (P399), in particular as those might be different for the three stations (TENATSO, St.308, St.311). Therefore, simulated temperature, salinity, and phytoplankton profiles in April and June are compared to observations taken during P399. At the TENATSO station and at St.308 temperature and salinity profiles are similar to the observed ones (Fig. A1a, b). The greatest mismatch occurs in the surface layer, where no restoring takes place. There, salinity and temperature are strongly influenced by vertical exchange via turbulence, surface fluxes (momentum, heat, radiation), which are a function of the forcing used. The forcing taken from climatological mean data can not fully represent local conditions during the cruise. Modelled nutrient profiles (Fig. A2d–e) at TENATSO and St.308 closely match observed ones. Modelled and observed phytoplankton biomass profiles (Fig. A2a–b) show similarities, but also significant differences. Similar to observations, the model predicts a subsurface phytoplankton maximum, but location and extent differ among the two stations and also compared to model results. Phytoplankton biomass is calculated from a depth-dependent C : Chl ratio. The ratio is derived from an empirical parameterization, which introduces uncertainities to the observations. A direct comparison of model results to measured phytoplankton pigments on the other hand is not possible, as chorophyll is not a prognostic variable of the model. Nevertheless, modelled and observation-based phytoplankton concentrations are in the same order of magitude and show a similar vertical profile.

At St.311 the shallower nutricline (Fig. A2f), a surface maximum of phytoplankton (Fig. A2c), lower surface water temperatures (Fig. A1f), and a lower salinity (Fig. A1c) indicate that the station could be influenced by coastal upwelling. Upwelling

BGD
10, 1111–1145, 2013

off Mauretania and Senegal is strongest in winter (January–April) and weakens during the northward displacement of the Intertropical Convergence Zone (i.e. until late summer), and the associated surface phytoplankton bloom persists until summer (Sawadogo et al., 2009). This bloom stretches from the coast offshore, hence it is possible that St.311 that is close to the coast is influenced by these coastal processes whereas the other stations are not. As the 1-D water colum model GOTM is not able to reproduce wind-driven coastal upwelling, which constitutes an advective process, CH_3I observations from St.311 will not be included in the evaluation of the model.

Acknowledgements. The authors are grateful to Helmke Hepach (Geomar, Helmholtz Center for Ocean Reseach Kiel) for providing CH_3I concentrations and to Ilka Peeken (Alfred Wegener Institute for Polar and Marine Research, Bremerhaven) for providing phytoplankton pigment data from the Poseidon Cruise P399. The study was funded by the German BMBF project SOPRAN (Surface Ocean Processes in the Anthropocene) SOPRAN I 03F0462E, SOPRAN II 03F0611E; IH is financed through the Cluster of Excellence "CliSAP" (EXC177), University of Hamburg, funded through the German Science Foundation (DFG).

References

Agusti, S.: Viability and niche segregation of Prochlorococcus and Synechococcus cells across the Central Atlantic Ocean, Aquat. Microb. Ecol., 36, 53–59, 2004. 1117, 1128

Bange, H.: FS Poseidon Fahrtbericht/Cruise Report P399 – 2 & 3: Eastern tropical North Atlantic; P399-2: 31.04.2010–17.06.2010 Las Palmas – Las Palmas (Canary Islands), P399-3: 18.–24.06.2010 Las Palmas (Canary Islands) – Vigo (Spain); DRIVE (Diurnal and Reglonal Variability of Halogen Emmissions), SOPRAN, Cruise Report 10.3289/ifm-geomar_rep_48_2011, IfM-Geomar Kiel, Kiel, available at: http://oceanrep.geomar.de/12032/, 2011. 1122, 1128

Bell, N., Hsu, L., Jacob, D., Schultz, M., Blake, D., Butler, J., King, D., Lobert, J., and Maier-Reimer, E.: Methyl iodide: atmospheric budget and use as a tracer of marine convection in global models, J. Geophys. Res., 107, 4340, doi:10.1029/2001JD001151, 2002 1113

BGD
10, 1111–1145, 2013

Brownell, D., Moore, R., and Cullen, J.: Production of methyl halides by *Prochlorococcus* and *Synechococcus*, Global Biogeochem. Cy., 24, GB2002, doi:10.1029/2009GB003671, 2010. 1113
Carlson, C.: Biogeochemistry of marine dissolved organic matter, chap. Production and removal processes, 91–152, Academic Press, An Elsevier Science Imprint, 2002. 1115, 1116
Carpenter, L. and Liss, P.: On temperate sources of bromoform and other reactive organic bromine gases, J. Geophys. Res.-Atmos., 105, 20539–20547, 2000. 1119
Chameides, W. and Davis, D.: Iodine: its possible role in tropospheric photochemistry, J. Geophys. Res., 85, 7383–7398, 1980. 1112
Chuck, A., Turner, S., and Liss, P.: Oceanic distributions and air-sea fluxes of biogenic halocarbons in the open ocean, J. Geophys. Res.-Oceans, 110, 1–12, 2005. 1129
Conkright, M. E., Locarnini, R. A., Garcia, H. E., O'Brien, T. D., Boyer, T. P., Stephens, C., and Antonov, J. I.: World Ocean Atlas 2001: Objective Analyses, Data Statistics, and Figures, CDROM Documentation, Tech. rep., National Oceanographic Data Center, Silver Spring, MD, USA, 2002. 1120, 1128
Dittmar, W.: Part I: report on researches into the composition of ocean-water, collected by H.M.S. Challenger, during the years 1873–1876, Phys. Chem., 1, 1–247, 1884. 1118
Elliott, S. and Rowland, F.: Nucleophilic substitution rates and solubilities for methyl halides in seawater, Geophys. Res. Lett., 20, 1043–1046, 1993. 1118
Elliott, S. and Rowland, F.: Methyl halide hydrolysis rates in natural waters, J. Atmos. Chem., 20, 229–236, 1995. 1119
Happell, J. and Wallace, D.: Methyl iodide in the Greenland/Norwegian Seas and the tropical Atlantic Ocean: evidence for photochemical production, Geophys. Res. Lett., 23, 2105–2108, 1996. 1129
Hense, I. and Beckmann, A.: Revisiting subsurface chlorophyll and phytoplankton distributions, Deep-Sea Res. Part I, 55, 1193–1199, 2008. 1122
Hense, I. and Quack, B.: Modelling the vertical distribution of bromoform in the upper water column of the tropical Atlantic Ocean, Biogeosciences, 6, 535–544, doi:10.5194/bg-6-535-2009, 2009. 1116, 1117, 1120
Hughes, C., Franklin, D., and Malin, G.: Iodomethane production by two important marine cyanobacteria: *Prochlorococcus marinus* (CCMP 2389) and *Synechococcus sp.* (CCMP 2370), Mar. Chem., 125, 19–25, 2011. 1113, 1117, 1128

BGD
10, 1111–1145, 2013

Lovelock, J., Maggs, R., and Wade, R.: Halogenated hydrocarbons in and over the Atlantic [8], Nature, 241, 194–196, 1973. 1112
Moore, R.: Methyl halide production and loss rates in sea water from field incubation experiments, Mar. Chem., 101, 213–219, 2006. 1113
Moore, R. and Groszko, W.: Methyl iodide distribution in the ocean and fluxes to the atmosphere, J. Geophys. Res.-Oceans, 104, 11163–11171, doi:10.1029/1998JC900073, 1999. 1120
Moore, R., Geen, C., and Tait, V.: Determination of Henry's law constants for a suite of naturally occurring halogenated methanes in seawater, Chemosphere, 30, 1183–1191, 1995. 1120
Moore, R., Webb, M., Tokarczyk, R., and Wever, R.: Bromoperoxidase and iodoperoxidase enzymes and production of halogenated methanes in marine diatom cultures, J. Geophys. Res.-Oceans, 101, 20899–20908, 1996. 1116, 1121, 1128, 1130
Nightingale, P., Malin, G., and Liss, P.: Production of chloroform and other low-molecular-weight halocarbons by some species of macroalgae, Limnol. Oceanogr., 40, 680–689, 1995. 1112
Nightingale, P. D., Malin, G., Law, C., Watson, A., Liss, P., Liddicoat, M., Boutin, J., and Upstill-Goddard, R.: In situ evaluation of airsea gas exchange parameterizations using novel conservative and volatile tracers, Global Biogeochem. Cy., 14, 373–387, 2000. 1119
O'Brien, L. M., Harris, N. R. P., Robinson, A. D., Gostlow, B., Warwick, N., Yang, X., and Pyle, J. A.: Bromocarbons in the tropical marine boundary layer at the Cape Verde Observatory – measurements and modelling, Atmos. Chem. Phys., 9, 9083–9099, doi:10.5194/acp-9-9083-2009, 2009. 1121
Partensky, F., Hess, W., and Vaulot, D.: *Prochlorococcus*, a marine photosynthetic prokaryote of global significance, Microbiol. Mol. Biol. R., 63, 106–127, 1999. 1117
Rattigan, O., Shallcross, D., and Cox, R.: UV absorption cross-sections and atmospheric photolysis rates of CF_3I, CH_3I, C_2H_5I and CH_2ICl, J. Chem. Soc. Faraday T., 93, 2839–2846, 1997. 1119
Richter, U. and Wallace, D.: Production of methyl iodide in the tropical Atlantic Ocean, Geophys. Res. Lett., 31, 1–4, 2004. 1113, 1129
Sawadogo, S., Brajard, J., Niang, A., Lathuiliere, C., Crepón, M., and Thiria, S.: Analysis of the Senegalo-Mauritanian Upwelling by processing satellite remote sensing observations with topological maps, Proceedings of International Joint Conference on Neural Networks, Atlanta, Georgia, USA, 14–19 June, 2826–2832, 2009. 1132

BGD
10, 1111–1145, 2013

Six, K. and Maier-Reimer, E.: Effects of plankton dynamics on seasonal carbon fluxes in an ocean general circulation model, Global Biogeochem. Cy., 10, 559–583, 1996. 1114
Smythe-Wright, D., Boswell, S., Breithaupt, P., Davidson, R., Dimmer, C., and Eiras Diaz, L.: Methyl iodide production in the ocean: Implications for climate change, Global Biogeochem. Cy., 20, GB3003, doi:10.1029/2005GB002642, 2006. 1113, 1116, 1121, 1128, 1129, 1130
Sulzberger, B. and Durisch-Kaiser, E.: Chemical characterization of dissolved organic matter (DOM): a prererquisite for understanding UV-induced changes of DOM absorption properties and bioavailabilty, Aquat. Sci., 71, 104–126, 2009. 1115
Umlauf, L., Burchard, H., and Bolding, K.: GOTM – scientific documentation: version 3.2, Mar. Sci. Rep., 63, 1–346, 2005. 1114
Wallace, D. R. and Bange, H.: Introduction to special section: results of the Meteor 55: tropical SOLAS expedition, Geophys. Res. Lett., 31, L23S01, doi:10.1029/2004GL021014, 2004. 1127
Wang, L., Moore, R., and Cullen, J.: Methyl iodide in the NW Atlantic: spatial and seasonal variation, J. Geophys. Res.-Oceans, 114, C07007, doi:10.1029/2007JC004626, 2009. 1112
Weber, L., Völker, C., Oschlies, A., and Burchard, H.: Iron profiles and speciation of the upper water column at the Bermuda Atlantic Time-series Study site: a model based sensitivity study, Biogeosciences, 4, 689–706, doi:10.5194/bg-4-689-2007, 2007. 1120
Wetzel, P., Maier-Reimer, E., Botzet, M., Jungclaus, J., Keenlyside, N., and Latif, M.: Effects of ocean biology on the penetrative radiation in a coupled climate model, J. Climate, 19, 3973–3987, 2006. 1114

BGD
10, 1111–1145, 2013

Table 1. Parameter setup of the NPZD model, default HAMOCC values and new values after tuning to fit observations close to Cape Verde.

Parameter	Default value	New value
Phytoplankton mortality rate (water column)[d^{-1}]	0.1	0.3
Grazing rate [d^{-1}]	1.0	0.7
Initial slope of the *P-I* curve [$d^{-1}\,(W\,m^{-2})^{-1}$]	0.02	0.025
Phytoplankton half saturation rate [kmol P m^{-3}]	1.0×10^{-8}	4.0×10^{-8}

BGD
10, 1111–1145, 2013

Table 2. CH_3I model parameter configurations of the different experiments. The unit of k_{PP} is [mmol CH_3I (kmol P)$^{-1}$], the one of k_{photo} is [m^2 mmol CH_3I (kmol P)$^{-1}$ W^{-1} s^{-1}].

Experiment ID	$k_{PP_{(min)}}$	$k_{PP_{max}}$	k_{photo} (SLDOC)	k_{photo} (RDOC)
E1	0.1232	0.0	0.0	0.0
E2	1488.00	0.0	0.0	0.0
E3	0.1232	1488.00	0.0	0.0
Opt1	56.00	0.0	0.0	0.0
Opt2	0.0	0.0	1.31×10^{-6}	0.0
Opt3	0.0	0.0	0.0	3.91×10^{-7}
Opt4	0.144	1204.8	0.0	0.0
Opt123	0.045	0.0	7.80×10^{-7}	1.26×10^{-7}

BGD
10, 1111–1145, 2013

Table 3. Observed and modelled concentrations at the surface, concentration minima and maxima [pmol L^{-1}]. Modelled values are means of the respective months at the depth of the observations.

	Maximum		Mean		Surface	
Experiment ID	TENATSO	Stat.308	TENATSO	Stat.308	TENATSO	Stat.308
E1	0.11	0.14	0.02	0.004	0.11	0.14
E2	173.20	187.65	60.67	70.43	28.64	38.16
E3	6.24	5.67	1.23	1.57	6.24	5.55
Opt1	6.52	7.08	2.30	2.68	1.18	1.57
Opt2	5.60	5.04	2.00	2.31	4.66	4.65
Opt3	5.36	4.98	2.14	2.46	4.52	4.37
Opt4	5.34	4.94	1.08	1.39	5.34	4.83
Opt123	5.07	4.62	1.89	2.18	4.24	4.19
Observation	5.66	3.34	1.49	0.66	0.06	0.9

BGD
10, 1111–1145, 2013

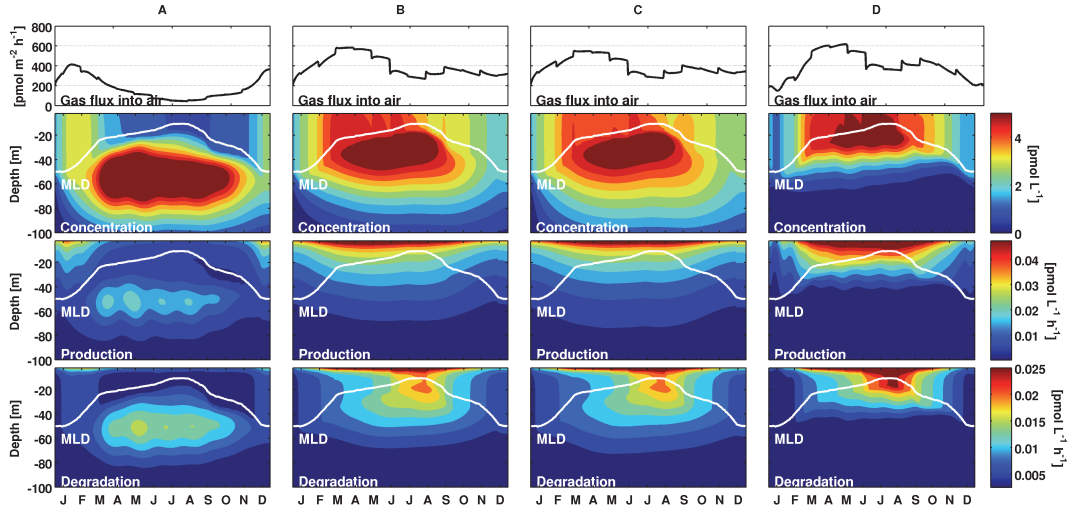

Fig. 1. Methyl iodide concentrations [pmol L^{-1}], production [pmol L^{-1} h^{-1}], degradation [pmol L^{-1} h^{-1}], gas exchange [pmol m^{-2} h^{-1}] for the experiments Opt1 (column **A**), Opt2 (column **B**), Opt3 (column **C**), and Opt4 (column **D**).

BGD
10, 1111–1145, 2013

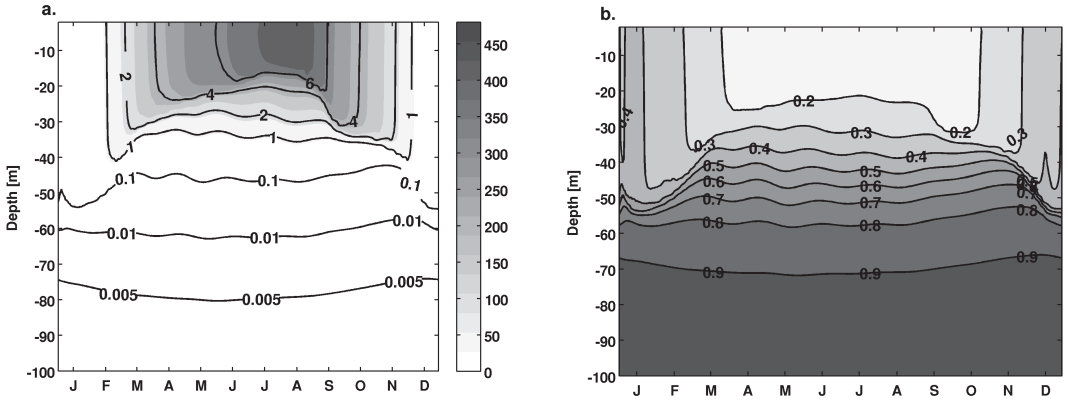

Fig. 2. Ratio between methyl iodide and primary production rate k_{PP} in Opt4 (a, gray shaded, [mmol CH_3I (kmol P)$^{-1}$]), its relation to k_{PP} in Opt1 (i.e. $\frac{k_{PP_{Opt4}}}{k_{PP_{Opt1}}}$) (**a**, contour lines), and the nutrient limitation factor N_{lim} **(b)**.

BGD
10, 1111–1145, 2013

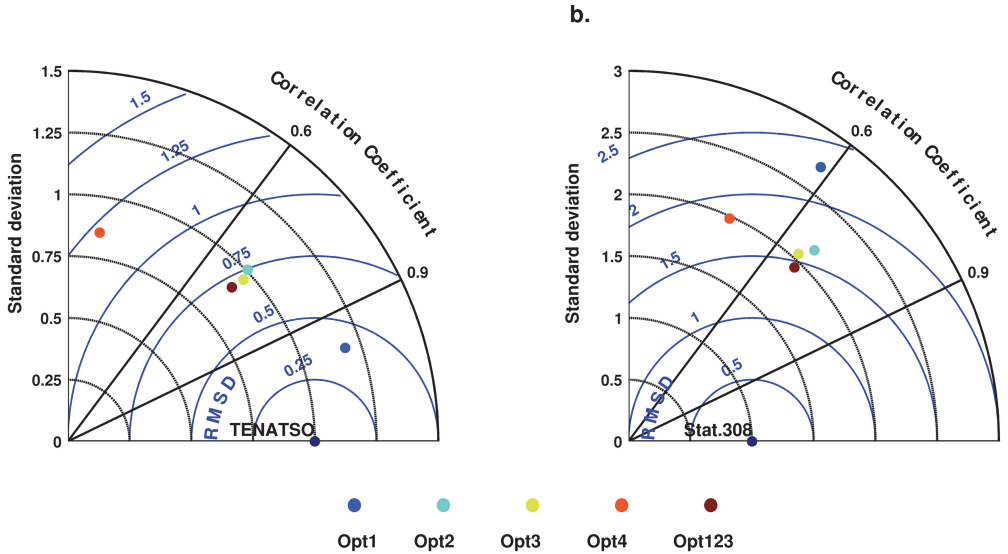

Fig. 3. Taylor diagrams for the different experiments showing the RMSD between modelled and observed profiles normalized with the observed mean concentration (blue circles), standard deviations of the individual profiles normalized with the one of the observations (black circles, ticks on the y-axis), and the linear correlation coefficient between model results and observations (angle between y- and x-axis). Note, all statistical parameters are derived from the vertical profiles, not from a time series. Observations are from TENATSO **(a)** and St.308. **(b)**.

BGD
10, 1111–1145, 2013

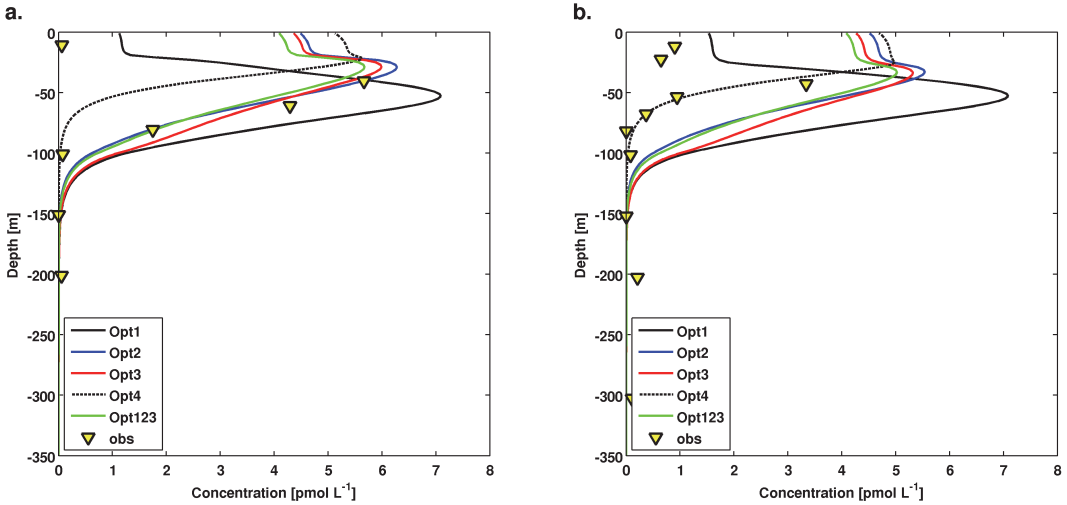

Fig. 4. Methyl iodide concentration profiles [pmol L^{-1}] from stations TENATSO and St.308 in the Cape Verde region. Observed data were collected during Poseidon cruise P399/2 in 2010. For the Tenatso station only data from the upper 350 m of the water column are shown.

BGD
10, 1111–1145, 2013

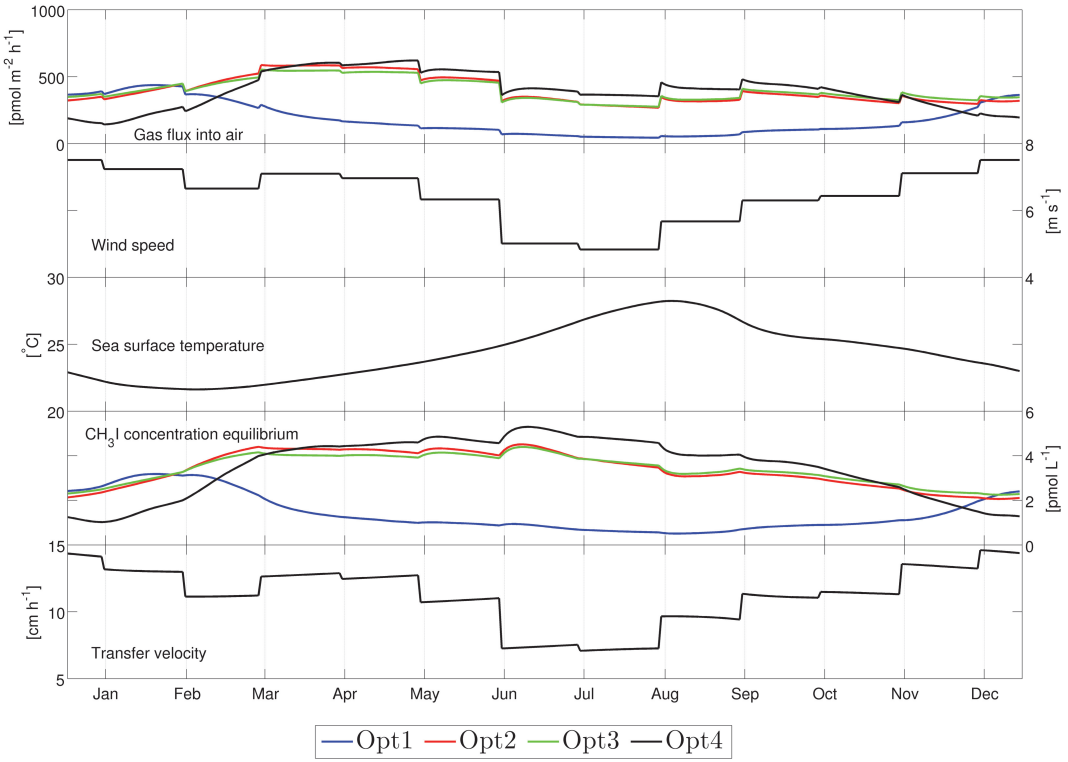

Fig. 5. Methyl iodide sea-air flux [pmol m^{-2} h^{-1}], wind speed [m s^{-1}], sea surface temperature [°C], CH_3I water and air concentration equilibrium ($c_w - \frac{c_a}{H}$, [pmol L^{-1}]), and gas transfer velocity [cm h^{-1}].

BGD
10, 1111–1145, 2013

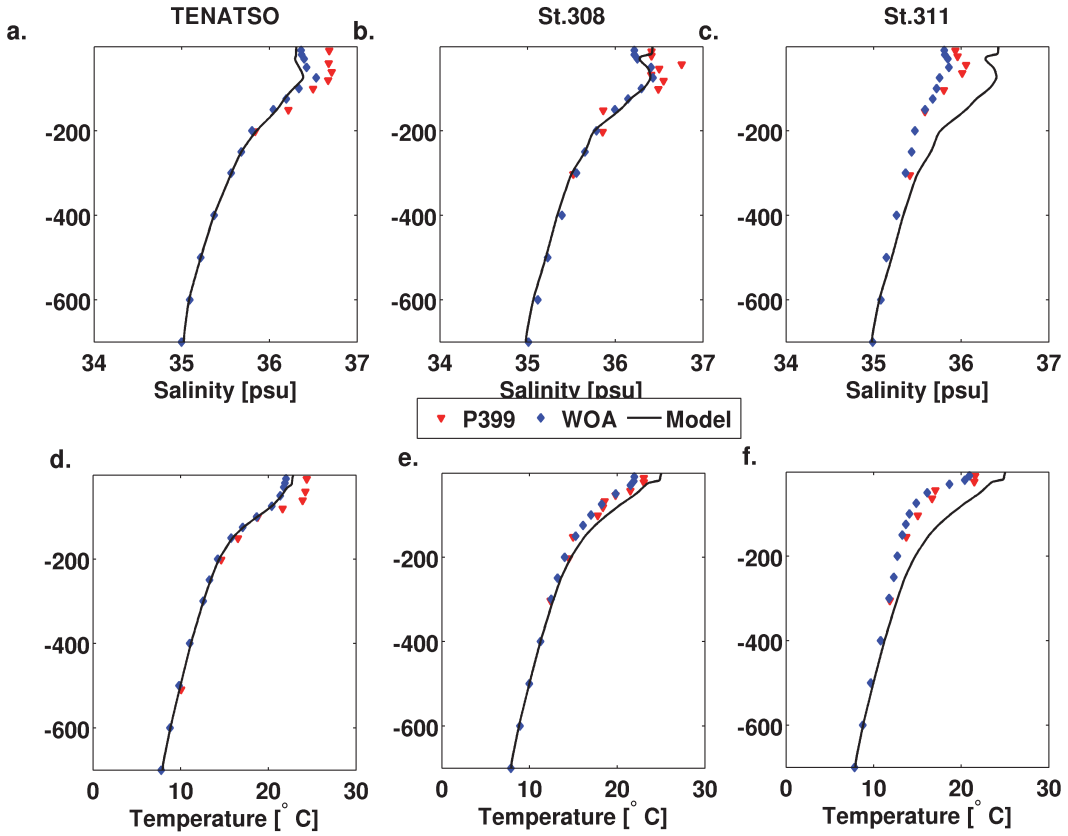

Fig. A1. Salinity [psu] **(a–c)** and temperature [°C] **(d–f)** profiles in April **(a, d)** and June **(b, c, e, f)**, model predicted (solid lines) and observations (red markers P399 cruise data, blue markers WOA data).

BGD
10, 1111–1145, 2013

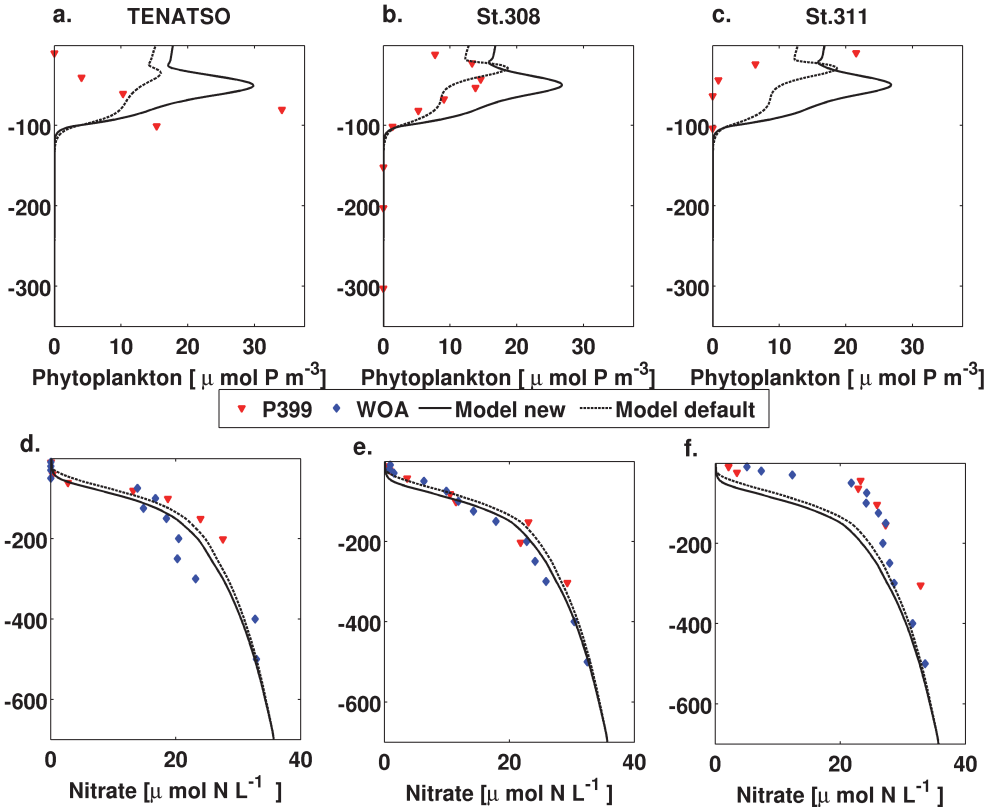

Fig. A2. Phytoplankton **(a–c)** and nutrient **(d–f)** concentrations in April **(a, d)** and June **(b, c, e, f)** [μmol P m^{-3}], model predicted (black solid lines new and dashed lines default parameter setup) and observed (red markers) profiles. Observations were taken from the Poseidon Cruise P399 in 2010. Phytoplankton concentrations have been derived from chlorophyll, using a vertically dependent C : Chl-ratio (e.g. Hense and Beckmann, 2008) and the Redfield ratio for conversion from carbon to nitrogen.

BGD
10, 1111–1145, 2013